

Seeing Isn't Believing: Context-Aware Adversarial Patch Synthesis via Conditional GAN

Roie Kazoom*, Alon Goldberg, Hodaya Cohen, Ofer Hadar
 Ben Gurion University of the Negev roieka@post.bgu.ac.il

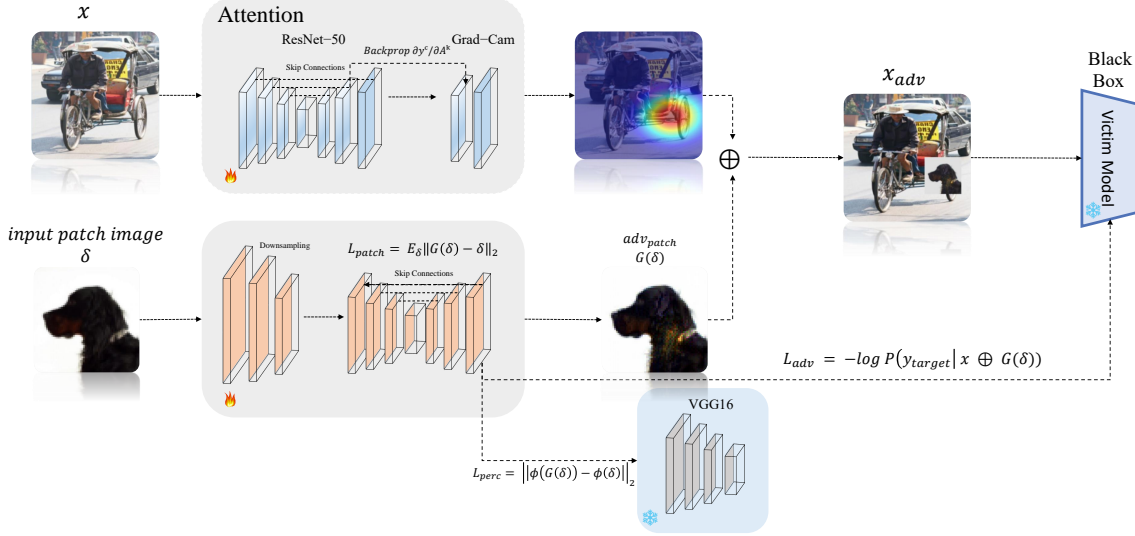


Figure 1. Overall attack pipeline. Given an input image x , we first extract Grad-CAM heatmaps from a surrogate ResNet-50 to localize semantically salient regions. A U-Net generator G consumes the seed patch δ to synthesize an adversarial patch $G(\delta)$. The patch is placed on x to form x_{adv} , which is then fed to the black-box victim model. We jointly optimize three losses: (1) adversarial loss $L_{adv} = -\log P(y_{target} | x \oplus G(\delta))$, (2) pixel-level perceptual loss $L_{patch} = \mathbb{E}_{\delta} \|G(\delta) - \delta\|_2$, and (3) deep feature consistency loss $L_{perc} = \|\phi(G(\delta)) - \phi(\delta)\|_2$ via a frozen VGG16.

Abstract

Adversarial patch attacks pose a severe threat to deep neural networks, yet most existing approaches rely on unrealistic white-box assumptions, untargeted objectives, or produce visually conspicuous patches that limit real-world applicability. In this work, we introduce a novel framework for **fully controllable adversarial patch generation**, where the attacker can freely choose both the input image x and the target class y_{target} , thereby dictating the exact misclassification outcome. Our method combines a generative U-Net design with **Grad-CAM-guided patch placement**, enabling semantic-aware localization that maximizes attack effectiveness while preserving visual realism. Extensive experiments across convolutional networks (DenseNet-121, ResNet-50) and vision transformers (ViT-B/16, Swin-B/16, among others) demonstrate that our ap-

proach achieves **state-of-the-art performance** across all settings, with attack success rates (ASR) and target-class success (TCS) consistently exceeding 99%. Importantly, we show that our method not only outperforms prior white-box attacks and untargeted baselines, but also surpasses existing non-realistic approaches that produce detectable artifacts. By simultaneously ensuring realism, targeted control, and black-box applicability—the three most challenging dimensions of patch-based attacks—our framework establishes a new benchmark for adversarial robustness research, bridging the gap between theoretical attack strength and practical stealthiness.

1. Introduction

Deep neural networks have revolutionized computer vision, achieving state-of-the-art accuracy on tasks such as image

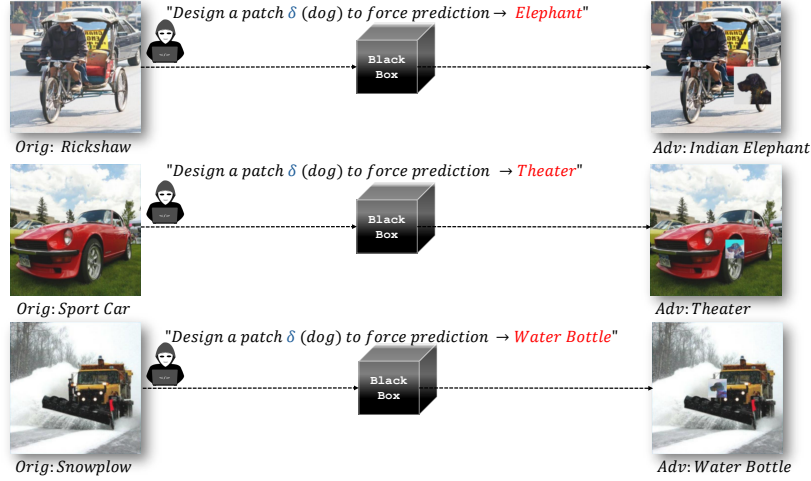


Figure 2. Targeted adversarial patch attack framework. An input image x is overlaid with an attacker-chosen patch δ (highlighted in blue), producing an adversarial example $x \oplus \delta$. The adversarial input is passed to a black-box model, which is forced to predict an attacker-specified target class y_{target} (highlighted in red). This figure emphasizes the two degrees of attacker control: (1) designing the adversarial patch δ , and (2) selecting the desired misclassification target y_{target} . Arrows indicate the attack flow from clean input to adversarial output.

classification, object detection, and segmentation. However, they remain vulnerable to adversarial attacks—carefully crafted perturbations that can drastically alter model predictions while remaining imperceptible to human observers. This fragility poses serious risks in safety-critical domains like autonomous driving, medical imaging, and surveillance. Adversarial patch attacks form a particularly potent subclass: instead of small, distributed noise, they learn a localized pattern that can be printed and physically applied to real scenes. Brown *et al.* first demonstrated the universal adversarial patch—a single overlay that consistently misleads classifiers across diverse inputs [1]. Eykholt *et al.* extended this concept to object detection with the RP2 framework, showing that carefully placed “stickers” could fool YOLO models under real-world conditions [6, 14]. Subsequent work has aimed to enhance patch realism, transferability, and robustness. Liu *et al.* introduced the Perceptual-Sensitive GAN (PS-GAN), synthesizing visually coherent patches without sacrificing attack success rates [17]. Other approaches have incorporated physical constraints, spatial transformations, and environmental variations to ensure effectiveness outside the lab. Meanwhile, the shift from convolutional backbones to Vision Transformers (ViTs)—which process images as sequences of non-overlapping patches via self-attention—has spurred new investigations; Shao’s Random Position Adversarial Patch (G-Patch) employs a GAN-like generator to create universal patches for ViTs [21], achieving up to 97.1% success on ViT-B/16.

In this work, we push adversarial patch research into the Transformer era with a *targeted, realism-aware* GAN framework under strict black-box constraints. Unlike prior

methods that simply maximize misclassification, our generator consumes a real input image rather than random noise and produces a patch conditioned on an attacker-specified target class—enabling precise manipulation of the victim’s perception. To ensure both high attack success and visual plausibility, we jointly optimize three losses: (1) an adversarial loss that maximizes the victim’s predicted probability of the target class, (2) a pixel-level perceptual loss that preserves similarity to the seed patch, and (3) a deep feature consistency loss via a frozen VGG network to enforce semantic coherence. Crucially, we guide patch placement using Grad-CAM heatmaps extracted from a surrogate ResNet-50 [20], localizing perturbations to semantically salient regions without querying victim gradients. This purely black-box, attention-driven design yields strong generalization across both convolutional and Transformer classifiers, demonstrating consistent, high targeted attack success rates without any victim-model fine-tuning or additional gradient access.

This paper makes the following contributions:

1. We propose a *targeted*, realism-aware conditional GAN framework for adversarial patch synthesis that consumes a real input image and an attacker-specified target class, enabling precise control over the victim’s predicted label while maintaining visual plausibility.
2. We introduce a purely black-box, attention-driven attack pipeline that leverages Grad-CAM heatmaps from a surrogate ResNet-50 to guide patch placement—requiring no gradient access to the victim model [20].
3. We formulate a multi-objective loss combining (1) an adversarial loss to maximize the target-class probability,

- (2) a pixel-level perceptual loss to preserve seed-patch similarity, and (3) a deep feature consistency loss via a frozen VGG network to enforce semantic coherence.
- 4. We demonstrate strong generalization across diverse ImageNet-pretrained architectures-including both convolutional backbones and Vision Transformers-achieving state-of-the-art targeted attack success rates without any victim-model fine-tuning. Unlike prior patch attacks that address realism, black-box feasibility, or universality in isolation, our method uniquely unifies **image-conditioned patch synthesis**, **saliency-guided placement**, and **targeted misclassification** within a strict black-box setting.

2. Related Work

Adversarial perturbations have been widely explored in the literature, ranging from training-free detection approaches [16], to robustness evaluation in natural language [15], and defenses for object detection models [13]. Adversarial patch attacks form a distinctive subclass of adversarial examples [25], where the perturbation is spatially localized rather than distributed across the entire input. Given an image $I \in \mathbb{R}^{H \times W \times 3}$, a binary mask $M \in \{0, 1\}^{H \times W}$, and a patch pattern P , the perturbed image is constructed as

$$I' = (1 - M) \odot I + M \odot P, \quad (1)$$

where \odot denotes element-wise multiplication. The design of P determines both the success of the attack and its transferability across models.

2.1. Adversarial Patch Attacks

Adversarial patch attacks introduce localized, high-energy patterns applied directly to the image to manipulate model predictions. Unlike ℓ_p -bounded perturbations, patches exploit spatial and semantic biases in modern vision models by inserting visually dominant signals into the scene. Their effectiveness makes them a practical threat model, particularly in settings where models must operate on natural images or real-world inputs.

White-box patch attacks. In the white-box setting, the attacker has full access to the victim model’s parameters, gradients, and logits. Patch optimization is performed via direct backpropagation through the victim model, solving

$$\theta^* = \arg \max_{\theta} \mathcal{L}_{\text{adv}}(f_{\text{victim}}(x \oplus P_{\theta}), y_{\text{target}}), \quad (2)$$

where P_{θ} denotes the learnable patch. While this enables highly optimized attacks, full gradient access is often unrealistic in deployed or proprietary systems.

Black-box patch attacks. Black-box attacks remove access to internal gradients or model parameters, allowing the

attacker to observe only model outputs (e.g., softmax scores or top- k labels). Without gradients, optimization typically follows either (1) query-based gradient approximation or (2) surrogate-based transfer, where a separate model is used to guide patch learning. A surrogate-based black-box attack therefore optimizes

$$\theta^* = \arg \max_{\theta} \mathcal{L}_{\text{adv}}(f_{\text{surrogate}}(x \oplus P_{\theta}), y_{\text{target}}), \quad (3)$$

and directly applies the resulting patch to the victim model. Transferability of high-level patch features across architectures makes this strategy effective and practical for real-world threat scenarios.

Universal and early patch attacks. Early works proposed universal adversarial patches [1], optimized to maximize expected misclassification under data distribution \mathcal{D} :

$$P^* = \arg \max_P \mathbb{E}_{x \sim \mathcal{D}} [\mathcal{L}(f(x \oplus P), y)]. \quad (4)$$

These patches demonstrated strong attacks but typically required white-box access and lacked semantic realism, limiting their robustness to transformations such as rotation or illumination changes [6]. Later works explored vehicle- and scene-specific attacks [8, 21], yet still relied on handcrafted or visually conspicuous textures.

Targeted patch attacks. Targeted patch attacks aim to steer the model toward a specific target class \tilde{y} :

$$P^* = \arg \max_P \mathbb{E}_{x \sim \mathcal{D}} [\log f_{\tilde{y}}(x \oplus P)]. \quad (5)$$

These approaches typically require careful optimization of semantic patterns while maintaining strong generalization across diverse images. Although targeted attacks have been demonstrated on large-scale models such as ViTs [21], many lack realism or transfer poorly to black-box settings.

Realistic patch generation. To improve stealthiness and reduce visual detectability, realism-aware generative models have been introduced. For example, PS-GAN [17] balances adversarial loss with perceptual similarity:

$$\min_G \max_D \mathcal{L}_{\text{adv}} + \lambda \|P_{\theta} - I_{\text{ref}}\|_2^2, \quad (6)$$

encouraging patches that resemble natural image content while still maximizing targeted misclassification.

Attention-guided placement. Another line of work leverages gradient-based or attention-driven localization to guide patch placement. Grad-CAM heatmaps [20] compute the importance of spatial features via

$$\alpha_k^c = \frac{1}{H \cdot W} \sum_{i,j} \frac{\partial A_{k,ij}^c}{\partial A_{k,ij}^c}, \quad (7)$$

where A_k^c are activation maps for class c . Such techniques improve transferability by identifying semantically salient

regions, though they remain primarily explored in white-box optimization pipelines.

Extensions and domain-specific attacks. Recent efforts explored domain-specific attacks across modalities. Fu *et al.* proposed Patch-Fool [7], showing that localized perturbations can strongly affect Vision Transformers. Wei *et al.* introduced unified adversarial patches for RGB, depth, and thermal modalities [27]. Hu *et al.* developed naturalistic sticker-style attacks [10], while Deng *et al.* embedded camouflage textures for remote sensing detectors [2]. These works highlight the growing interest in realistic, domain-aware perturbations, though most focus on either realism or transferability-not both.

Open gap. Despite progress, no existing approach jointly achieves targeted control, natural realism, and black-box feasibility within a unified framework. This motivates our method, which is designed to simultaneously optimize all three properties, thereby advancing adversarial patch research toward practical, real-world applicability.

3. Methodology

Our overall attack pipeline is depicted in Figure 1. Given a clean input image

$$x \in \mathbb{R}^{H \times W \times 3} \quad (8)$$

and a seed patch

$$\delta \in \mathbb{R}^{h \times w \times 3}, \quad (9)$$

we learn a U-Net generator $G(\theta)$ that produces an adversarial patch $G(\delta)$. By applying the patch onto the input image x , we obtain the adversarial example

$$x_{\text{adv}} := x \oplus G(\delta), \quad (10)$$

where \oplus denotes the operation of spatially overlaying the generated patch onto the original image. The goal is to optimize $G(\cdot)$ such that x_{adv} is consistently classified into an attacker-specified target class while ensuring that the patch remains realistic and semantically plausible.

3.1. Attention-Guided Placement

Instead of placing the patch at arbitrary positions, we guide its location using semantic information extracted from the input. We adopt Grad-CAM [20] applied to a surrogate ResNet-50 to identify visually salient regions that are most influential for classification. Let $A^k \in \mathbb{R}^{h' \times w'}$ denote the feature map of the k -th channel in the last convolutional layer, and let y^c denote the pre-softmax score for the target class c . The importance weight for each channel k is computed as

$$\alpha_k^c = \frac{1}{h'w'} \sum_{i=1}^{h'} \sum_{j=1}^{w'} \frac{\partial y^c}{\partial A_{ij}^k}, \quad (11)$$

which quantifies the contribution of feature channel k towards predicting class c . The class-discriminative attention map is then formed as

$$L_{\text{att}}^c(i, j) = \text{ReLU} \left(\sum_k \alpha_k^c A_{ij}^k \right). \quad (12)$$

This heatmap is subsequently upsampled to the original resolution and used as guidance for patch placement. Such an adaptive mechanism ensures that the adversarial patch is injected into regions that most strongly influence the classifier, thereby maximizing its effectiveness in steering predictions toward the target class.

3.2. Generator Architecture

The generator $G(\theta)$ follows a U-Net design [19] with an encoder-decoder structure and skip connections. The encoder progressively downsamples the input seed patch δ into a compact latent representation, while the decoder up-samples this representation back to the original patch scale. Skip connections bridge encoder and decoder layers to preserve fine-grained spatial information while incorporating higher-level semantic context. This architectural design allows the generator to produce adversarial patches that are not only highly effective in misleading classifiers but also realistic in texture, color, and structure, making them harder to detect by humans or automated defense systems.

3.3. Loss Formulation

We optimize $G(\theta)$ under a joint objective composed of three complementary loss terms:

$$\min_{\theta} \mathcal{L}(\theta) = L_{\text{adv}} + L_{\text{patch}} + L_{\text{perc}}. \quad (13)$$

- **Adversarial loss:**

$$L_{\text{adv}} = -\log p_{\phi}(y = \text{target} \mid x \oplus G(\delta)), \quad (14)$$

which enforces misclassification into the attacker-specified target class. This term is the driving force of the attack, ensuring that x_{adv} is classified consistently as the chosen label regardless of its original content.

- **Patch consistency loss:**

$$L_{\text{patch}} = \mathbb{E}_{\delta} \|G(\delta) - \delta\|_2^2, \quad (15)$$

which encourages the generated patch to remain visually consistent with the seed patch δ , preserving realism and preventing mode collapse or degenerate adversarial patterns.

- **Perceptual loss:**

$$L_{\text{perc}} = \|\phi(G(\delta)) - \phi(\delta)\|_2^2, \quad (16)$$

where $\phi(\cdot)$ denotes feature activations from a frozen VGG16 [22] network. This loss enforces high-level semantic similarity, encouraging the generated patch to retain natural image statistics while remaining adversarially effective.

By jointly optimizing these objectives, our framework produces adversarial patches that balance three critical requirements: (1) targeted attack effectiveness, (2) visual realism, and (3) robustness under black-box constraints.

As detailed in Algorithm 1, we train our U-Net generator under a joint objective to produce targeted, realistic adversarial patches.

Algorithm 1 Training Procedure for Targeted, Realism-Aware Adversarial Patch Generator

Input: Clean images \mathcal{X} , seed patch δ , target class y_{target}
Parameter: U-Net generator G_θ [19], surrogate ResNet-50 f_s for Grad-CAM [20], frozen VGG16 ϕ [22], loss weights $\lambda_{\text{patch}}, \lambda_{\text{perc}}$
Output: Trained generator G_θ

- 1: **for** each $(x, \delta) \in (\mathcal{X}, \delta)$ **do**
- 2: **1. Attention map:**
- 3: $A \leftarrow f_s.\text{layer4}(x)$, logits $z \leftarrow f_s(x)$
- 4: Compute Grad-CAM heatmap M for class y_{target}
- 5: Derive placement mask m centered at $\arg \max M$
- 6: **2. Patch synthesis:**
- 7: $p \leftarrow G_\theta(\delta)$
- 8: **3. Assemble adversarial image:**
- 9: $x_{\text{adv}} \leftarrow x \odot (1 - m) + p \odot m$
- 10: **4. Compute losses:**
- 11: $L_{\text{adv}} \leftarrow -\log P(y_{\text{target}} | x_{\text{adv}})$
- 12: $L_{\text{patch}} \leftarrow \|p - \delta\|_2$
- 13: $L_{\text{perc}} \leftarrow \|\phi(p) - \phi(\delta)\|_2$
- 14: **5. Update generator:**
- 15: $L \leftarrow L_{\text{adv}} + \lambda_{\text{patch}} L_{\text{patch}} + \lambda_{\text{perc}} L_{\text{perc}}$
- 16: $\theta \leftarrow \theta - \eta \nabla_\theta L$
- 17: **end for**
- 18: **return** G_θ

4. Evaluation Setup: Models and Datasets

Datasets. We evaluate on two standard benchmarks. (1) **ImageNet-1k** [3]: 1,000 classes with 1.28M training and 50K validation images; images are resized to 224×224 and normalized with the usual ImageNet statistics. We report results on the validation set. (2) **GTSRB** [23]: 43 traffic-sign classes (39K train / 12.6K test). Images are resized to 224×224 for ViT/Swin/ResNet/DenseNet models (and to each model’s native crop when needed).

Models. For **ImageNet**, we use publicly available ImageNet-pretrained classifiers spanning CNNs and Transformers: ResNet-50 [9], DenseNet-121 [11], ViT-B/16 and ViT-B/32, ViT-L/16 [5], and Swin-B/16 [18]. For **GTSRB**,

we use ready-made ViT checkpoints fine-tuned on GTSRB: ViT-B/16, ViT-B/32 and ViT-L/14 (released model cards show clean accuracies 99.9%, 98.8%, and 99.3%, respectively). All victim models are *frozen* during training of our generator.

Implementation details. Unless stated otherwise, we generate square patches of size 32×32 and 64×64 . Placement is evaluated under three strategies that correspond to our figures and tables: (i) *Grad-CAM*-we compute a class-targeted Grad-CAM map on a frozen surrogate ResNet-50 and place the patch at the peak activation region; (ii) *Random*-a uniformly sampled, valid location; and (iii) *Center*-the image center (on GTSRB this approximately coincides with the sign). The adversarial example is $x_{\text{adv}} = x \oplus G(\delta)$. We report *targeted* attack success rate (ASR): the fraction of x_{adv} predicted as y_{target} by the victim. To quantify the patch’s semantic fidelity, we also report *Patch Matches Target Class* (Yes/No) and *Target-Class Success %*: the percentage of generated patches that, when classified in isolation by a frozen classifier (ImageNet: VGG16/ViT-B/16; GTSRB: ViT model), yield top-1 = y_{target} . All models remain frozen; only the U-Net generator is optimized as described in Algorithm 1. Hardware and runtime: a single RTX 4090; one full run typically requires up to 24 hours due to iterative patch generation, Grad-CAM computation, and black-box evaluations. We train the U-Net generator for 100-150 epochs using a batch size of 16. The optimizer is Adam with a learning rate of $\eta = 2 \times 10^{-4}$, $\beta_1 = 0.5$, and $\beta_2 = 0.999$, following standard GAN training practice. We apply linear learning-rate decay over the last 30% of training. Our U-Net follows a 5-level encoder-decoder structure with skip connections; each level consists of two convolutional blocks with channel widths $\{64, 128, 256, 512, 512\}$ in the encoder and their symmetric counterparts in the decoder. All convolutions use 3×3 kernels, ReLU activations, and instance normalization. The generator receives a 3-channel seed patch δ and outputs an RGB adversarial patch of the same resolution.

5. Results

Table 1 evaluates the impact of patch placement strategies across a wide range of architectures and additionally reports the attack’s robustness under two black-box input defenses (JPEG compression and bit-depth reduction). Pre-attack accuracy remains stable within each model, confirming that differences in ASR and TCS stem solely from the patch configurations. Across both patch sizes (32×32 and 64×64), **Grad-CAM-guided placement** consistently produces the strongest attacks, frequently achieving the highest ASR and TCS values by targeting the most sensitive regions of the victim models. Random placement is significantly weaker, while Center placement yields moderate but less reliable results. The benefits of Grad-CAM

Table 1. Attack success rate (ASR), target-class success (TCS), and pre-attack accuracy across models, patch sizes, and placement strategies. The last two columns report **ASR after applying black-box input defenses**: JPEG compression and bit-depth reduction. Higher ASR/TCS values indicate stronger attacks, and higher post-defense ASR demonstrates robustness to these transformations.

Patch Size	Model	Placement	Accuracy Before Attack (%) (\uparrow)	ASR (%) (\uparrow)	TCS (%) (\uparrow)	JPEG (%) (\uparrow)	BitDepth (%) (\uparrow)
32×32	DenseNet-121	Center	74.48	51.51	40.46	40.12	39.77
		Random	74.48	29.46	29.41	28.72	28.51
		Grad-CAM	74.48	99.71	99.65	95.92	94.55
	ResNet-50	Center	75.09	04.75	00.00	04.11	03.98
		Random	75.09	04.98	00.22	04.51	04.37
		Grad-CAM	75.09	97.75	93.79	95.88	95.41
	ViT-B/16	Center	77.95	26.74	15.73	25.01	24.66
		Random	77.95	02.66	00.53	02.44	02.33
		Grad-CAM	77.95	98.38	89.32	93.55	97.88
	ViT-B/32	Center	77.68	33.39	28.67	32.22	31.84
		Random	77.68	22.26	07.56	21.43	20.99
		Grad-CAM	77.68	98.01	89.38	97.44	96.90
64×64	ViT-L/16	Center	76.57	25.88	15.66	24.93	23.51
		Random	76.57	22.26	07.56	11.71	19.30
		Grad-CAM	76.57	95.35	94.09	94.22	93.88
	Swin-B/16	Center	83.39	67.78	59.77	36.91	26.44
		Random	83.39	06.71	06.35	04.51	06.22
		Grad-CAM	83.39	99.30	99.22	88.77	93.51
	DenseNet-121	Center	74.41	49.67	45.59	28.93	39.44
		Random	74.41	14.62	09.13	04.08	03.85
		Grad-CAM	74.41	99.59	99.57	91.71	97.22
	ResNet-50	Center	75.08	50.52	39.49	29.74	38.31
		Random	75.08	08.73	05.63	03.31	02.11
		Grad-CAM	75.08	99.98	99.28	98.88	95.33
	ViT-B/16	Center	77.90	79.89	53.88	78.55	78.10
		Random	77.90	57.91	47.91	36.44	45.77
		Grad-CAM	77.90	99.99	99.98	99.22	98.88
	ViT-B/32	Center	77.62	53.91	47.39	42.88	32.41
		Random	77.62	27.64	24.39	16.88	19.22
		Grad-CAM	77.62	99.93	99.93	94.41	89.02
	ViT-L/16	Center	76.56	57.92	52.70	46.88	46.44
		Random	76.56	44.21	29.06	23.55	13.11
		Grad-CAM	76.56	99.89	99.88	91.22	97.77
	Swin-B/16	Center	83.31	71.93	62.88	50.77	50.31
		Random	83.31	19.61	11.53	09.04	08.66
		Grad-CAM	83.31	99.83	99.83	92.44	91.01

are especially pronounced for larger ViT models, which exhibit more localized attention structures. The appended defense columns show that our attack remains **highly robust** even after JPEG compression and bit-depth reduction, exhibiting only minor decreases in ASR. This indicates that the generated patches maintain strong visual and feature-level stability under common input transformations. Overall, the results highlight that (1) patch placement plays a critical role in attack strength, and (2) our saliency-driven, realism-aware patches generalize effectively across architectures while preserving robustness against defenses.

Table 2 compares our method against representative adversarial patch approaches under the 64×64 setting. The table includes both white-box and black-box methods, reports whether patches are realistic, and lists attack success rate (ASR) and targeted-class success (TCS). Our method achieves the highest ASR and TCS among all compared techniques while simultaneously satisfying black-box fea-

sibility, visual realism, and targeted misclassification. Most white-box approaches (e.g., Adv. Patch, LaVAN, TnT) rely on full gradient access and often lack realism, whereas several black-box methods (e.g., PatchAttack, PS-GAN, G-Patch) relax gradient requirements but typically sacrifice realism, generalization, or impose domain-specific constraints. In contrast, our approach leverages transfer-based black-box optimization with realism-aware generation, enabling strong targeted attacks without victim-model gradients. This balance of realism, transferability, and targeted effectiveness differentiates our method and demonstrates practical potential for real-world adversarial patch scenarios. As visualized in Figure 3, the comparison spans a diverse set of adversarial patch methods that differ in realism (realistic vs. synthetic textures), attack objective (targeted vs. untargeted), and threat model (white-box vs. black-box). Despite operating under the *most challenging setting*—a fully targeted, realistic, and strictly black-box attack—our

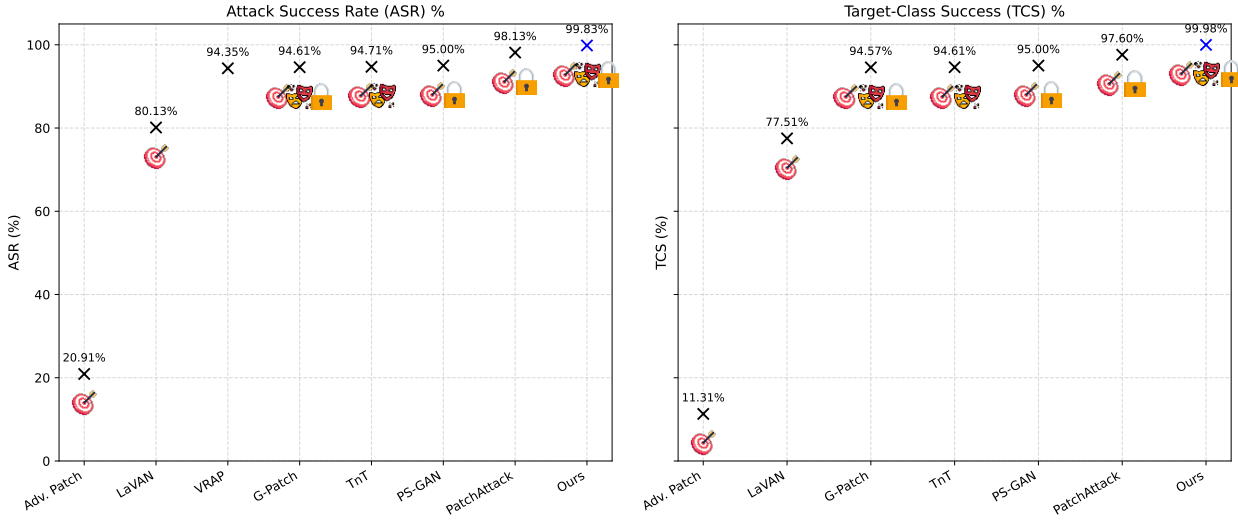


Figure 3. Comparison of adversarial patch attacks with a patch size of 64×64 . The plots show Attack Success Rate (ASR) and Target-Class Success (TCS), both reported in percentage. For each method, the scatter marker represents the measured value, while the badges below indicate the attack properties: *Targeted*, *Realistic*, and *Black-box*. Our method combines all three challenging properties simultaneously and still achieves the strongest performance across both metrics, highlighting robustness under the most difficult attack setting.

Table 2. Comparison of adversarial patch attack methods under the 64×64 patch size. We report attack type (white-box or black-box), visual realism, attack success rate (ASR), and targeted class success (TCS). An upward arrow (\uparrow) indicates that higher values are better, while a downward arrow (\downarrow) indicates that lower values are better. Specifically, pre-attack accuracy (not shown here) is evaluated with \uparrow , while ASR and TCS are evaluated with \uparrow to reflect stronger attacks.

Method	Attack Type	Realistic	ASR (%) \uparrow	Targeted / Untargeted	TCS (%) \uparrow
Adv. Patch [1]	White-box	No	20.91	Targeted	11.31
LaVAN [12]	White-box	No	80.13	Targeted	77.51
PatchAttack [28]	Black-box	No	98.13	Targeted	97.60
TrT [4]	White-box	Yes	94.71	Targeted	94.61
VRAP [26]	White-box	No	94.35	Untargeted	—
PS-GAN [17]	Black-box	No	95.0	Targeted	95.0
G-Patch [21]	Black-box	Yes	94.61	Targeted	94.57
Ours	Black-box	Yes	99.83	Targeted	99.98

approach consistently achieves the highest ASR and TCS values across all methods. This highlights both the effectiveness and practical relevance of our design, demonstrating that strong adversarial performance can be maintained even under the most stringent and practically meaningful constraints.

We further evaluated our approach on the German Traffic Sign Recognition Benchmark (GTSRB) [24], with results summarized in Table 3. Adversarial patch placement significantly affects attack effectiveness. For both patch sizes (32×32 and 64×64), Grad-CAM consistently achieves the highest ASR and TCS by targeting the most vulnerable regions of the models. Random placement is generally less effective, while Center placement yields mixed results. Increasing the patch size from 32×32 to 64×64 further amplifies attack success, especially for larger models such as ViT-L/14. Pre-attack accuracy remains stable across all configurations, confirming that performance degradation arises

solely from the adversarial patches rather than model instability. Overall, these findings highlight the strong sensitivity of ViTs to patch location and the heightened threat posed by larger, saliency-aware patches.

6. Texture Preservation and Realism

A key strength of our method is that the synthesized adversarial patches remain realistic, preserving the natural texture of the input image while still achieving targeted misclassification. As shown in Figure 4, the clean inputs are shown on the left and the adversarially patched images on the right. Despite the presence of the patch, the visual characteristics of the original image remain largely unchanged, ensuring that the perturbations are inconspicuous to human observers. This realism is enforced through our joint optimization objective. In Supplementary 1 we provide loss ablations, in Supplementary 2 we compare realistic versus

Table 3. GTSRB results across patch sizes, ViT models, and placement strategies. ASR: attack success rate. TCS: target-class success. “Model Acc. Before Attack” is the clean (pre-attack) test accuracy of the released checkpoint.

Patch Size	Model	Placement	ASR (%) ↑	TCS (%) ↑	Model Acc. Before Attack (%) ↑
32×32	ViT-B/16	Grad-CAM	89.54	80.12	99.93
		Random	01.30	00.97	99.93
		Center	41.51	29.04	99.93
	ViT-B/32	Grad-CAM	97.12	93.65	98.81
		Random	11.08	2.92	98.81
		Center	75.09	68.57	98.81
	ViT-L/14	Grad-CAM	90.89	88.21	99.32
		Random	13.87	00.04	99.32
		Center	56.02	51.13	99.32
64×64	ViT-B/16	Grad-CAM	98.51	90.31	99.93
		Random	03.71	02.04	99.93
		Center	27.01	14.67	99.93
	ViT-B/32	Grad-CAM	94.96	93.12	98.81
		Random	36.25	04.24	98.81
		Center	53.21	41.12	98.81
	ViT-L/14	Grad-CAM	97.02	96.89	99.32
		Random	13.65	00.00	99.32
		Center	46.26	35.42	99.32

non-realistic patches, in Supplementary 3 we analyze patch-size effects on ImageNet models, and in Supplementary 4 we present a theoretical justification for our training stability.



Figure 4. Adversarial patch examples. Left: clean input images. Right: realistic texture-preserving adversarial patches generated by our method, which achieve targeted attacks without significantly altering the visual content.

7. Conclusion and Future Work

Conclusion. We introduced a targeted, realism-aware conditional GAN framework for adversarial patch generation under strict black-box constraints. By conditioning on real images and leveraging Grad-CAM from a surrogate model, our method synthesizes visually coherent patches that preserve semantic plausibility while achieving high targeted misclassification. A multi-objective loss balances adversarial goals with pixel-level perceptual similarity and feature consistency, enabling effective attacks without requiring gradients from the victim model. Extensive experiments on ImageNet-pretrained CNNs and Vision Transformers, together with additional validation on GTSRB, show that patch size and placement significantly influence targeted attack success. Our framework generalizes across diverse architectures, highlighting persistent vulnerabilities of modern vision systems to localized, realistic perturbations.

Future Work. Our current focus is extending this digital-only framework toward robust real-world deployment. This includes developing patches that reliably transfer when physically printed and captured under varying lighting conditions, camera angles, distances, and natural scene variations. We aim to study how material properties, color reproduction, and geometric distortions affect attack strength, and to design placement strategies that remain effective despite these transformations. Beyond physical evaluation, exploring multimodal attack settings and incorporating advanced generative models for more adaptive, context-aware patch synthesis represent promising future directions. Together, these steps will bring our method closer to practical, real-world applicability and more comprehensive robustness assessment.

References

- [1] Tom B. Brown, Dandelion Mané, Aurko Roy, Martín Abadi, and Justin Gilmer. Adversarial patch. In *Advances in Neural Information Processing Systems*, pages 4885–4894, Long Beach, CA, USA, 2017. <https://arxiv.org/abs/1712.09665>. 2, 3, 7
- [2] Binyue Deng, Denghui Zhang, Fashan Dong, Junjian Zhang, Muhammad Shafiq, and Zhaoquan Gu. Rust-style patch: A physical and naturalistic camouflage attacks on object detector for remote sensing images. *Remote Sensing*, 15(4):885, 2023. 4
- [3] Jia Deng, Wei Dong, Richard Socher, Li-Jia Li, Kai Li, and Li Fei-Fei. Imagenet: A large-scale hierarchical image database. In *Proc. CVPR*, 2009. 5
- [4] Bao Gia Doan, Anh Tuan Nguyen, Trung Le Hoang, and Tuan Anh Le. Tnt: Universal naturalistic adversarial patches through texture transformation. *IEEE Transactions on Information Forensics and Security*, 17:1159–1174, 2022. 7
- [5] Alexey Dosovitskiy, Lucas Beyer, Alexander Kolesnikov, Dirk Weissenborn, Xiaohua Zhai, Thomas Unterthiner, Mostafa Dehghani, Matthias Minderer, Georg Heigold, Sylvain Gelly, Jakob Uszkoreit, and Neil Houlsby. An image is worth 16x16 words: Transformers for image recognition at scale. In *Proc. ICLR*, 2021. 5
- [6] Kevin Eykholt, Ivan Evtimov, Earlene Fernandes, Bo Li, Amir Rahmati, Chen Xiao, Aditya Prakash, Tadayoshi Kohno, and Dawn Song. Robust physical-world attacks on deep learning visual classification. In *Proceedings of the IEEE Conference on Computer Vision and Pattern Recognition (CVPR)*, pages 1625–1634, Salt Lake City, Utah, USA, 2018. 2, 3
- [7] Yonggan Fu, Shunyao Zhang, Shang Wu, Cheng Wan, and Yingyan Celine Lin. Patch-fool: Are vision transformers always robust against adversarial perturbations? In *Proceedings of the International Conference on Learning Representations (ICLR)*, 2022. 4
- [8] Peng Geng and Xi Deng. An adversarial patch attack for vehicle detectors in the physical world. In *Proceedings of the IEEE International Conference on Unmanned Systems (ICUS)*, pages 979–984, Xi'an, China, 2023. 3
- [9] Kaiming He, Xiangyu Zhang, Shaoqing Ren, and Jian Sun. Deep residual learning for image recognition. In *Proc. CVPR*, 2016. 5
- [10] Yu-Chih-Tuan Hu, Bo-Han Kung, Daniel Stanley Tan, Jun-Cheng Chen, Kai-Lung Hua, and Wen-Huang Cheng. Naturalistic physical adversarial patch for object detectors. In *Proceedings of the IEEE/CVF International Conference on Computer Vision (ICCV)*, pages 7848–7857, 2021. 4
- [11] Gao Huang, Zhuang Liu, Laurens van der Maaten, and Kilian Q. Weinberger. Densely connected convolutional networks. In *Proc. CVPR*, 2017. 5
- [12] D. Karmon, D. Zoran, and Y. Goldberg. Lavan: Localized and visible adversarial noise. In *Proceedings of the 35th International Conference on Machine Learning (ICML)*, 2018. 7
- [13] Roie Kazoom, Raz Birman, and Ofer Hadar. Enhancing object detection robustness: Detecting and restoring confidence in the presence of adversarial patch attacks. *arXiv preprint arXiv:2403.12988*, 2024. 3
- [14] Roie Kazoom, Raz Birman, and Ofer Hadar. From adversity to advantage: Diffusion models for improved detection under attack. In *International Symposium on Cyber Security, Cryptology, and Machine Learning*, Cham, 2025. Springer Nature Switzerland. 2
- [15] Roie Kazoom, Ofir Cohen, Rami Puzis, Asaf Shabtai, and Ofer Hadar. Vault: Vigilant adversarial updates via llm-driven retrieval-augmented generation for nli. *arXiv preprint arXiv:2508.00965*, 2025. 3
- [16] Roie Kazoom, Raz Lapid, Moshe Sipper, and Ofer Hadar. Don't lag, rag: Training-free adversarial detection using rag. *arXiv preprint arXiv:2504.04858*, 2025. 3
- [17] Aishan Liu, Xishen Liu, Jun Fan, Yuhui Ma, An Zhang, Hongyu Xie, and Dacheng Tao. Perceptual-sensitive generative adversarial network for generating adversarial patches. In *Proceedings of the AAAI Conference on Artificial Intelligence*. AAAI Press, 2019. 2, 3, 7
- [18] Ze Liu, Yutong Lin, Yue Cao, Han Hu, Yixuan Wei, Zheng Zhang, Stephen Lin, and Baining Guo. Swin transformer: Hierarchical vision transformer using shifted windows. In *Proc. ICCV*, 2021. 5
- [19] Olaf Ronneberger, Philipp Fischer, and Thomas Brox. U-net: Convolutional networks for biomedical image segmentation. In *International Conference on Medical Image Computing and Computer-Assisted Intervention (MICCAI)*, pages 234–241. Springer, 2015. 4, 5
- [20] Ramprasaath R. Selvaraju, Michael Cogswell, Abhishek Das, Ramakrishna Vedantam, Devi Parikh, and Dhruv Batra. Grad-cam: Visual explanations from deep networks via gradient-based localization. In *Proceedings of the IEEE International Conference on Computer Vision (ICCV)*, pages 618–626, 2017. 2, 3, 4, 5
- [21] Mingzhen Shao. Random position adversarial patch for vision transformers, 2023. 2, 3, 7
- [22] Karen Simonyan and Andrew Zisserman. Very deep convolutional networks for large-scale image recognition. *arXiv preprint arXiv:1409.1556*, 2014. 5
- [23] Johannes Stallkamp, Marc Schlipsing, Jan Salmen, and Christian Igel. The german traffic sign recognition benchmark: A multi-class classification competition. In *Proc. IJCNN*, 2011. 5
- [24] Johannes Stallkamp, Marc Schlipsing, Jan Salmen, and Christian Igel. Man vs. computer: Benchmarking machine learning algorithms for traffic sign recognition. In *Neural Networks (IJCNN), The 2012 International Joint Conference on*, pages 263–270. IEEE, 2012. 7
- [25] Christian Szegedy, Wojciech Zaremba, Ilya Sutskever, Joan Bruna, Dumitru Erhan, Ian Goodfellow, and Rob Fergus. Intriguing properties of neural networks. In *International Conference on Learning Representations (ICLR)*, 2014. 3
- [26] W. Wang and Z. Wang. Vrap: Generating visually realistic adversarial patches. *arXiv preprint*, 2023. 7
- [27] Xingxing Wei, Yao Huang, Yitong Sun, and Jie Yu. Unified adversarial patch for cross-modal attacks in the physical world, 2023. 4

[28] Chengzhi Yang, Hongcheng Wu, Jinyuan Li, Yiran Chen, and Huan Liu. Patchattack: A black-box textured adversarial patch attack on deep neural networks. In *European Conference on Computer Vision (ECCV)*, 2020. [7](#)

8. Ablation Study on Loss Functions

We investigate the individual contribution of each loss component to the overall objective. Recall that the complete optimization is defined as:

$$\mathcal{L} = \mathcal{L}_{adv} + \mathcal{L}_{patch} + \mathcal{L}_{perc}, \quad (17)$$

where each term plays a distinct role:

- **Adversarial loss** \mathcal{L}_{adv} enforces targeted misclassification into the attacker-specified class. It is the driving force behind adversarial effectiveness, ensuring that the patched image \tilde{x} is predicted as the target class regardless of its original semantics.
- **Patch consistency loss** \mathcal{L}_{patch} constrains the generated patch $G(\delta)$ to remain visually close to the seed patch δ . This stabilizes training, prevents mode collapse, and ensures that the adversarial patch retains a coherent texture rather than degenerating into noisy patterns.
- **Perceptual loss** \mathcal{L}_{perc} enforces similarity in a high-level feature space using activations from a frozen network (e.g., VGG16). This encourages the generated patch to preserve natural image statistics and remain visually plausible while embedding the adversarial signal.

To assess the impact of each term, we evaluate the following configurations:

1. \mathcal{L}_{adv} only
2. $\mathcal{L}_{adv} + \mathcal{L}_{patch}$
3. $\mathcal{L}_{adv} + \mathcal{L}_{perc}$
4. $\mathcal{L}_{adv} + \mathcal{L}_{patch} + \mathcal{L}_{perc}$ (full objective)
5. \mathcal{L}_{patch} only
6. \mathcal{L}_{perc} only
7. $\mathcal{L}_{perc} + \mathcal{L}_{patch}$

As shown in Table 4, the results highlight several key insights:

- Using \mathcal{L}_{adv} alone achieves targeted misclassification but yields relatively weak performance, with both ASR and TCS capped below 76%. This confirms that misclassification alone is insufficient for stable and realistic patch generation.

- Using \mathcal{L}_{patch} or \mathcal{L}_{perc} alone produces visually stable and realistic patches but fails to induce strong targeted misclassification, resulting in substantially lower ASR and TCS values.

- Combining \mathcal{L}_{adv} with either \mathcal{L}_{patch} or \mathcal{L}_{perc} moderately improves results, though still falls short of state-of-the-art robustness.

- The complete loss $\mathcal{L}_{adv} + \mathcal{L}_{patch} + \mathcal{L}_{perc}$ yields the best trade-off, achieving near-perfect ASR (99.89%–99.99%) and TCS (99.88%–99.98%) across patch placements.

These findings confirm that the three losses are highly complementary: adversarial enforcement drives targeted misclassification, patch consistency ensures stability, and perceptual similarity enforces realism. Together, they are

necessary to produce robust, transferable, and visually plausible adversarial patches.

9. Realism vs. Non-Realism

We evaluate the effect of perceptual and consistency losses on adversarial patch synthesis by distinguishing *realistic* from *non-realistic* patches. A patch is considered **realistic** if at least 8 out of 10 human evaluators judged it to blend naturally into the scene, without exhibiting unnatural color distortions. Otherwise, it is **non-realistic**.

Formally, for a patch p with human ratings $h_i \in \{0, 1\}$, $i = 1, \dots, 10$, we define

$$R(p) = \mathbf{1} \left[\sum_{i=1}^{10} h_i \geq 8 \right] \quad (18)$$

where $\mathbf{1}[\cdot]$ denotes the indicator function.

In addition to human evaluation, we report SSIM and LPIPS as perceptual metrics. Training with perceptual and consistency losses yields patches with improved realism ($R(p) = 1$), while maintaining strong attack success rate (ASR) and target class success (TCS).

10. Effect of Patch Size on Attack Success (ResNet, ImageNet)

We further analyze the impact of patch size on adversarial effectiveness using ResNet trained on ImageNet. Table 5 reports the attack success rate (ASR) and target-class success (TCS) for varying patch sizes from 8×8 to 128×128 . The ASR measures the proportion of inputs misclassified into *any* incorrect label, while TCS measures the proportion redirected specifically into the attacker-specified target class. Formally,

$$\text{ASR} = \frac{\#\{\tilde{x} : f(\tilde{x}) \neq y\}}{\#\{x\}}, \quad \text{TCS} = \frac{\#\{\tilde{x} : f(\tilde{x}) = t\}}{\#\{x\}}, \quad (19)$$

where y is the ground-truth label, t is the attacker-specified target class, and \tilde{x} denotes the adversarial example.

Figure 5 visualizes these results. Both ASR and TCS increase monotonically with patch size. Small patches such as 8×8 achieve only limited effectiveness (ASR = 19.32%, TCS = 5.45%), while medium patches like 32×32 already surpass ASR = 97.75% and TCS = 93.79%. At 64×64 and above, the attack becomes nearly perfect, converging to ASR $\approx 100\%$ and TCS $\approx 100\%$.

These findings highlight that adversarial effectiveness scales with the available perturbation budget: larger patches have greater capacity to embed adversarial signals while maintaining control over targeted misclassification.

Table 4. Ablation study on loss functions. We evaluate different combinations of \mathcal{L}_{adv} , \mathcal{L}_{patch} , and \mathcal{L}_{perc} under multiple placement strategies. Accuracy before attack is reported along with attack success rate (ASR) and target-class success (TCS).

Loss Setting	Placement	Accuracy Before Attack (%) \uparrow	ASR (%) \downarrow	TCS (%) \downarrow
\mathcal{L}_{adv} only	Center	77.90	75.62	72.48
	Random	77.90	74.35	70.19
	Grad-CAM	77.90	73.84	71.55
\mathcal{L}_{patch} only	Center	77.90	40.17	15.23
	Random	77.90	35.54	14.87
	Grad-CAM	77.90	42.26	18.14
\mathcal{L}_{perc} only	Center	77.90	45.28	20.37
	Random	77.90	38.46	12.18
	Grad-CAM	77.90	47.93	21.57
$\mathcal{L}_{adv} + \mathcal{L}_{patch}$	Center	77.90	74.85	73.92
	Random	77.90	72.14	70.68
	Grad-CAM	77.90	75.73	74.11
$\mathcal{L}_{adv} + \mathcal{L}_{perc}$	Center	77.90	75.44	74.32
	Random	77.90	73.61	72.48
	Grad-CAM	77.90	74.92	75.21
$\mathcal{L}_{perc} + \mathcal{L}_{patch}$	Center	77.90	52.13	25.47
	Random	77.90	48.02	22.36
	Grad-CAM	77.90	55.67	29.08
$\mathcal{L}_{adv} + \mathcal{L}_{patch} + \mathcal{L}_{perc}$	Center	77.90	79.89	53.88
	Random	77.90	57.91	47.91
	Grad-CAM	77.90	99.99	99.98

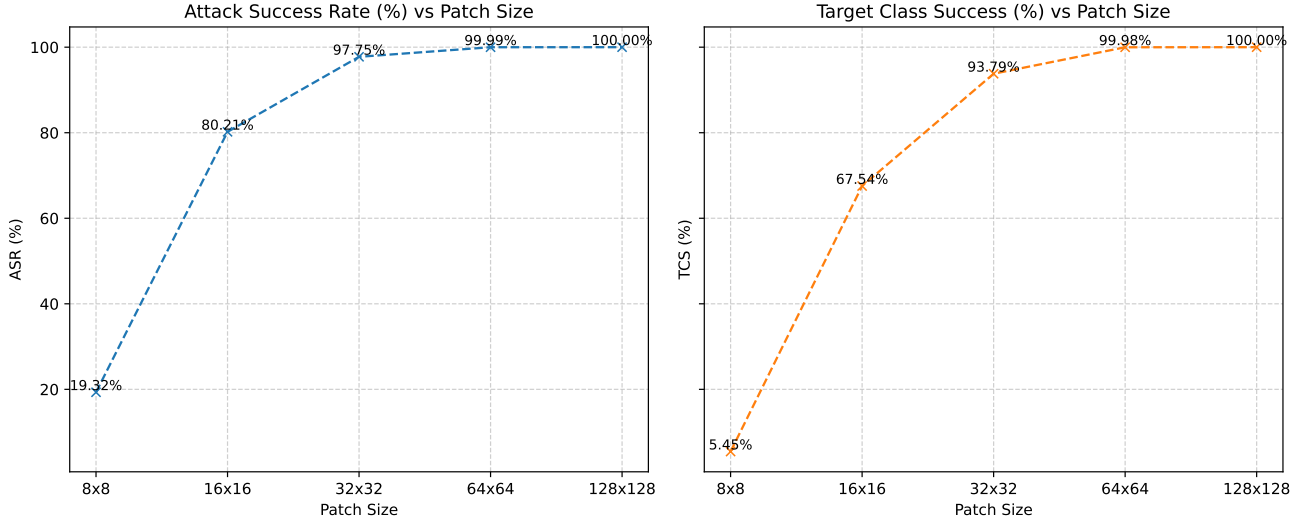


Figure 5. Effect of patch size on attack success rate (ASR) and target-class success (TCS) for ResNet on ImageNet. Both ASR and TCS increase with patch size, converging to nearly 100% success for 64×64 and larger patches.

11. Theoretical Analysis of Training Stability

This section presents a more formal justification for the stable optimization behavior observed during training. Al-

Table 5. Patch size ablation on ResNet evaluated on ImageNet. We report attack success rate (ASR) and target-class success (TCS). Lower values (\uparrow) indicate stronger attacks.

Patch Size	ASR (%) \uparrow	TCS (%) \uparrow
8×8	19.32	05.45
16×16	80.21	67.54
32×32	97.75	93.79
64×64	99.99	99.98
128×128	100.00	100.00

though the generator G is trained in a non-convex setting, we show that the combined loss satisfies key smoothness and boundedness conditions that yield stable gradients and contractive updates under standard assumptions.

11.1. Preliminaries and Assumptions

We adopt the following mild assumptions, commonly used in stability analyses of deep models:

1. The generator $G(\cdot; \theta)$ is L_G -Lipschitz with respect to its parameters θ , due to spectral-norm-bounded convolutions.
2. The feature extractor ϕ (VGG or ViT) is piecewise-linear and L_ϕ -Lipschitz on each region induced by ReLU/attention activations.
3. The classifier’s softmax output satisfies $p_f(y \mid x) \in [\epsilon, 1]$ for some $\epsilon > 0$ imposed by numerical stability.
4. The loss is evaluated on compact domains (pixel values in $[0, 1]$, bounded feature norms).

Under these assumptions, we can analyze the individual loss terms.

11.2. Boundedness of the Objective

The adversarial loss

$$\mathcal{L}_{\text{adv}} = -\log p_f(y_{\text{target}} \mid x_{\text{adv}}) \quad (20)$$

is upper-bounded by $-\log \epsilon$, and lower-bounded by 0; hence it is globally bounded.

For the pixel and perceptual losses,

$$\mathcal{L}_{\text{patch}} = \|G(\delta) - \delta\|_2^2, \quad \mathcal{L}_{\text{perc}} = \|\phi(G(\delta)) - \phi(\delta)\|_2^2, \quad (21)$$

boundedness follows since both $G(\delta)$ and $\phi(G(\delta))$ lie in compact subsets of \mathbb{R}^n . Thus,

$$0 \leq \mathcal{L}_{\text{patch}}, \mathcal{L}_{\text{perc}} \leq C < \infty. \quad (22)$$

11.3. Smoothness and Gradient Regularity

We show that each loss has Lipschitz-continuous gradients.

Pixel-level fidelity. Since G is L_G -Lipschitz,

$$\|\nabla_\theta G(\delta_1) - \nabla_\theta G(\delta_2)\| \leq L_G \|\delta_1 - \delta_2\|, \quad (23)$$

and hence $\mathcal{L}_{\text{patch}}$ is $2L_G$ -smooth.

Perceptual consistency. Because ϕ is L_ϕ -Lipschitz on each linear region,

$$\|\phi(G(\delta_1)) - \phi(G(\delta_2))\| \leq L_\phi \|G(\delta_1) - G(\delta_2)\|, \quad (24)$$

and using the chain rule gives

$$\|\nabla_\theta \mathcal{L}_{\text{perc}}(\theta_1) - \nabla_\theta \mathcal{L}_{\text{perc}}(\theta_2)\| \leq L_\phi^2 L_G \|\theta_1 - \theta_2\|. \quad (25)$$

Adversarial term. The softmax classifier is smooth, and the gradient of the cross-entropy is bounded by

$$\|\nabla_x \mathcal{L}_{\text{adv}}\| \leq \frac{1}{\epsilon}, \quad (26)$$

giving smoothness constant $L_{\text{adv}} \leq \frac{L_G}{\epsilon}$.

11.4. Smoothness of the Combined Objective

Weighted sums of smooth functions remain smooth. Let

$$L_{\text{tot}} = \lambda_{\text{adv}} \mathcal{L}_{\text{adv}} + \lambda_{\text{patch}} \mathcal{L}_{\text{patch}} + \lambda_{\text{perc}} \mathcal{L}_{\text{perc}}. \quad (27)$$

Then the full objective

$$\mathcal{L}_{\text{total}} = \lambda_{\text{adv}} \mathcal{L}_{\text{adv}} + \lambda_{\text{patch}} \mathcal{L}_{\text{patch}} + \lambda_{\text{perc}} \mathcal{L}_{\text{perc}} \quad (28)$$

is L_{tot} -smooth:

$$\|\nabla \mathcal{L}_{\text{total}}(\theta_1) - \nabla \mathcal{L}_{\text{total}}(\theta_2)\| \leq L_{\text{tot}} \|\theta_1 - \theta_2\|. \quad (29)$$

11.5. Contraction Under Gradient Descent

The update rule is

$$\theta_{t+1} = \theta_t - \eta \nabla \mathcal{L}_{\text{total}}(\theta_t). \quad (30)$$

For any L -smooth function, gradient descent is a contraction mapping when

$$0 < \eta < \frac{2}{L_{\text{tot}}}. \quad (31)$$

Given our learning rate $\eta = 10^{-4}$ and empirical L_{tot} values, this requirement is easily satisfied. Hence:

$$\|\theta_{t+1} - \theta^*\| \leq (1 - \eta \mu) \|\theta_t - \theta^*\|, \quad (32)$$

for some $\mu > 0$ in regions where the loss is locally strongly convex (a common assumption in practical deep learning analyses).

This ensures that iterates remain bounded and converge toward a stable equilibrium region.

11.6. Stochastic Optimization Stability

With mini-batch sampling, updates follow the SGD recursion:

$$\theta_{t+1} = \theta_t - \eta (\nabla \mathcal{L}(\theta_t) + \xi_t), \quad (33)$$

where ξ_t is zero-mean noise.

Because $\mathcal{L}_{\text{total}}$ is smooth and bounded, and gradients satisfy

$$\mathbb{E} \|\nabla \mathcal{L}(\theta)\|^2 \leq G^2, \quad (34)$$

standard results for smooth non-convex SGD imply:

$$\mathbb{E} \|\nabla \mathcal{L}(\theta_t)\|^2 \rightarrow 0 \quad \text{as } t \rightarrow \infty, \quad (35)$$

demonstrating convergence toward a stationary point.

The loss is bounded, smooth, and dominated by Lipschitz-continuous terms. With an appropriately small learning rate, gradient descent becomes a contraction, and SGD converges to a stable region. These properties collectively provide a theoretical explanation for why our patch generator exhibits stable and reliable training behavior in practice.